Modeling of Neuronal Population Activation under Electroconvulsive Therapy

Fadi N. Karameh[1], Mohamad Awada[1], Firas Mourad[1], Karim Zahed[1], Ibrahim Abou-Faycal[1] and Ziad Nahas [2]

[1]*Department of Electrical and Computer Engineering, American University of Beirut, 1107-2020, Beirut, Lebanon*

[2]*Department of Psychiatry, American University of Beirut Medical Center, 1107-2020, Beirut, Lebanon*

Keywords: Neuronal Modeling, EEG, Electroconvulsive Therapy, Kalman Filtering, Estimation.

Abstract: Electroconvulsive therapy (ECT) is a procedure that involves the induction of seizures in the brain of patients with severe psychiatric disorders. The efficacy and therapeutic outcome of electrically-induced seizures is dependent upon both the stimulus intensity and the electrode placement over the scalp, with potentially significant memory loss as side effect. Over the years, ECT modeling aimed to understand current propagation in the head medium with increasingly realistic geometry and conductivity descriptions. The utility of these models remain limited since seizure propagation in the active neural tissue has largely been ignored. Accordingly, a modeling framework that combines head conductivity models with active neural models to describe observed EEG signals under ECT is highly desirable. We present herein a simplified multi-area active neural model that describes (i) the transition from normal to seizure states under external stimuli with particular emphasis on disinhibition and (ii) the initiation and propagation of seizures between multiple connected brain areas. A simulation scenario is shown to qualitatively resemble clinical EEG recordings of ECT. Fitting model parameters is then performed using modern nonlinear state estimation approaches (cubature Kalman filters). Future work will integrate active models with passive volume conduction approaches to explore seizure induction and propagation.

1 INTRODUCTION

Electroconvulsive therapy (ECT) remains the most effective, and often lifesaving, acute treatment for severe psychiatric disorders. Each year, over 2 million treatments are administered world wide, but not without significant risks of memory loss.

Current ECT is commonly administered using two stimulating electrodes placed over the scalp of the patient under anesthesia. The location of the electrodes, the stimulus intensity and the stimulus duration are three main parameters that have been clinically linked to the focality and strength of the induced seizures. Here, the therapeutic benefit of an ECT session is related to the induction of prominent yet brief ($\sim$20 sec) seizures in the frontal areas of the brain followed by a period of marked inhibition, as observed in EEG recordings. Since electric current is injected at the scalp, there is little control over the nature and spatial extent of an induced seizure which is often global and can reach deeper structures in the brain related to memory formation and retention thus can adversely affect their normal operation. Accordingly, main recent thrust in ECT research has been focused on developing methods of delivery that can both retain seizure focality (and hence efficacy) and reduce its side effects. To this end, several ECT protocols have been introduced (Sackeim et al., 2008; Merkl et al., 2009). These differ mainly in the electrode location (bilateral, right/left unilateral, bifrontal), electrode shape and size (rectangular pads, circular), as well as electric stimulus shape (sinusoidal, unidirectional and bidirectional square waves) and duration (brief, ultra-brief).

At the earliest stages of protocol design, it is necessary to understand the excitatory implications (seizure strength and extent) of a given electrode-current configuration. Specifically, the affected brain areas can be implicated through *(i) primary excitation*, as determined by the electric field strength generated by the electrodes and the passive electric currents in the brain conductive medium, and *(ii) secondary excitation*, as determined by the active propagation of neuronal activity from one brain area to an-

N. Karameh F., Awada M., Mourad F., Zahed K., Abou-Faycal I. and Nahas Z..
Modeling of Neuronal Population Activation under Electroconvulsive Therapy.
DOI: 10.5220/0004804002290238
In *Proceedings of the International Conference on Bio-inspired Systems and Signal Processing* (BIOSIGNALS-2014), pages 229-238
ISBN: 978-989-758-011-6

other within the brain via inter-areal connections or pathways.

In this regard, simulation models can significantly enhance our understanding of a given electrode configuration and guide experimental testing. A principle challenge here is the introduction of stimulation protocols that preserve therapeutic efficacy of ECT seizures while reducing cognitive side effects. Several simulation models have been introduced to simulate the electric fields generated in head models with increasing realism starting from concentric spheres of homogenous conductivities to realistic detailed anatomical geometrical descriptions (such as those of the skull-sutures, plates etc.- and the brain surface-cortical sulci, corpus callosum etc.), with heterogenous conductivities (examples in (Deng et al., 2011; Lee et al., 2012),(Bai et al., 2012)). These models solve governing electrostatic equations over increasingly accurate domains, and produce electric field intensity profiles which are subsequently related to a given experimentally determined threshold of seizure initiation. Accordingly, such models primarily address primary excitation (point *(i)*) albeit with little or no attention given to secondary excitation, and hence are well suited to describe an initial operating point for seizure but not the dynamic spatiotemporal propagation of seizures, since the latter is dominated by the activity buildup and transport between brain areas (excessively synchronized firing in large scale neural populations).

Our approach advocates modeling ECT induced seizures initiation and propagation effected by both primary (passive) and secondary (active) excitation of brain tissue under scalp electrical stimulation. In this framework, the head-brain model is composed of two main simulation blocks as shown in figure 1. First, volume conduction is modeled to estimate the primary excitation arriving at the cortical surface due to input current stimulus at the scalp. Second, primary excitation arrives to underlying cortical structures whereby activating multi-area neural population models. The activity of these populations is then communicated between different areas thus producing secondary excitation. Finally, the model output is observed via EEG recordings at the scalp.

In this manuscript, we will focus on developing population models that could explain the induction of seizures within a local population due to exogenous currents such as that arriving from scalp stimuli (and hence is related to primary excitation), as well as propagating seizures across interconnected populations (hence is related to secondary excitation). The models will place a particular emphasis on the role of fast inhibition preceding seizure onset as a potential

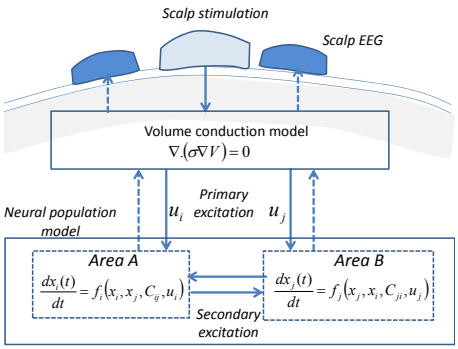

Figure 1: ECT modeling framework.

mechanism to reduce slow cortical inhibition and thus promote seizure induction. Subsequently, the parameters of the developed neural models will be estimated to qualitatively resemble clinical EEG recordings of ECT-induced seizures. Since the introduced models are nonlinear, state-of-the-art nonlinear Kalman filter estimation techniques are utilized to estimate both the neural activity of the underlying populations and the connectivity strength between corresponding brain areas thought to be implicated in seizure propagation.

2 NEURAL MODELS

The seizure generation models to be employed are intended to represent the genesis of ECT induced epileptic behavior both at the level of single area as well as at the level of multiple interacting areas. In this section we will initially present earlier models for spontaneous seizure initiation and subsequently introduce modifications to these models that allow exogenous seizure initiation in single (local) and multiple cortical areas.

2.1 Wendling Model

The single area neural population model is based on the work by Wendling et al (Wendling et al., 2002). This is a firing rate model with the basic neural firing element representing the main pyramidal cells that are reciprocally connected to local populations. The Wendling model, which is based on Jansen model(Jansen and Rit, 1995), is able to generate EEG like activity whose character depends on the set of connection parameters utilized.

In its simplest embodiments, the firing rate model of a single neural population is summarized by synaptic elements H_e, H_i representing excitatory and inhibitory connection of the population, and a sigmoidal current to rate transformation representing the neu-

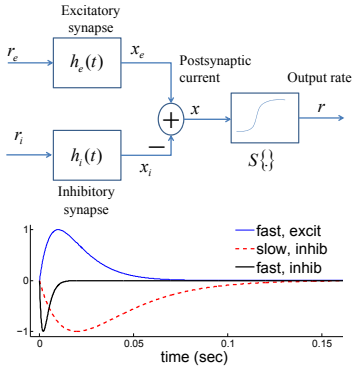

Figure 2: Neural population models. Top: Schematic of connectivity. Bottom: synaptic connections for fast excitatory, fast and slow inhibitory.

ral output (figure 2,top). A synapse H is thought of as a second order linear system whose impulse response follows a double-exponential (or alpha) function $h(t) = Aate^{-at}$. Accordingly, for a given input rate $r_i(t)$ arriving at this synapse, the synapse postsynaptic output current x(t) can be computed using a two-state linear system

$$\dot{x}(t) = z(t) \quad (1)$$

$$\dot{z}(t) = Aar_i(t) - 2az(t) - a^2x(t) \quad (2)$$

where z is an intermediate variable, a is the time constant for that synapse and A is an amplitude constant (values for these synaptic parameters used as in (Wendling et al., 2002)-see synaptic responses in figure 2, bottom). The population output is the firing rate which is produced after scaling and passing all synaptic currents through a static sigmoidal nonlinearity $r(t) = S\{cx(t)\}$, $S\{x\} = \frac{2e}{1+e^{k(x_o-x)}}$.

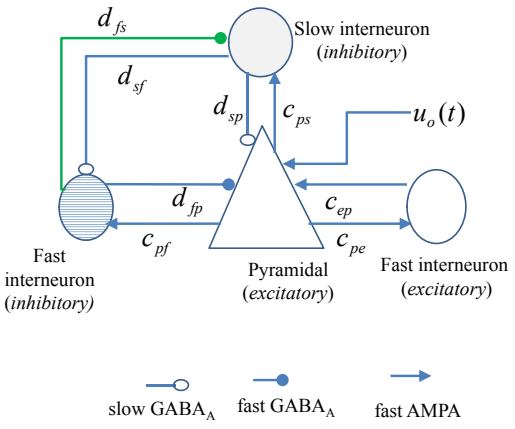

Figure 3: Local area model. Filled arrows represent fast excitatory connections ($h_e(t)$, time constant ~100 msec in figure 2); filled circles represent fast inhibitory connections ($h_i(t)$, time constant~20 msec), and hollow circles represent slow inhibitory connections ($h_i(t)$,time constant ~200 msec).

In extending the above basic neural population model to represent a the dynamics of a local cortical area, Wendling et al modeled the connectivity of pyramidal cells to three distinct interneuron populations that are thought to be widely present in cortical structures. As shown in the schematic of figure 3, the pyramidal cell population (triangles) are reciprocally connected to (i) a population of local excitatory interneurons that provide excitatory feedback to the pyramidal cells (ii) a population of fast inhibitory interneurons that provide fast GABA-A somatic inhibition, and (iii) a population of slow inhibitory interneurons that provide slow GABA-A dendritic inhibition. The corresponding extension of the neural population model (equation 1) results in the following set of nonlinear state-space equations:

$$\dot{x}_p(t) = z_1(t) \quad (3)$$

$$\dot{z}_1(t) = AaS\{x_e(t) - x_{is} - x_{if}(t)\} - 2az_p(t) - a^2x_p(t)$$

$$\dot{x}_e(t) = z_2(t) \quad (4)$$

$$\dot{z}_2(t) = Aa\left[u_0(t) + c_{ep}S\{c_{pe}x_p(t)\}\right] - 2az_2(t) - a^2x_e$$

$$\dot{x}_{is}(t) = z_3(t) \quad (5)$$

$$\dot{z}_3(t) = Bbd_{sp}S\{c_{ps}x_p(t)\} - 2bz_3(t) - b^2x_{is}$$

$$\dot{x}_{if}(t) = z_4(t) \quad (6)$$

$$\dot{z}_4(t) = Ggd_{fp}S\{c_{pf}x_p(t) - d_{sf}x_{ii}(t)\}) - 2gz_4(t) - g^2x_{if}$$

$$\dot{x}_{ii}(t) = z_5(t) \quad (7)$$

$$\dot{z}_5(t) = BbS\{c_{ps}x_p(t)\} - 2bz_5(t) - b^2x_{ii}(t)$$

$$e(t) = K_{iv}\left(x_e(t) - x_{is} - x_{if}(t)\right) \quad (8)$$

where $x_p(t)$ is the synaptic current output from pyramidal cell population to all local cells; x_e, x_{is}, and $x_{if}$are the excitatory input, slow ($GABA_A$ type) inhibitory input and fast ($GABA_A$ type) inhibitory input, respectively, to the pyramidal cells (refer to figure 3) ; x_{ii} is slow inhibitory input onto fast inhibitory cell. The constants (A,a), (B,b) and (G,g) dictate the time profiles of fast excitatory, slow inhibitory and fast inhibitory cells respectively (see figure 2, bottom). $u_0(t)$ is an external input assumed to arrive as a firing rate to the local pyramidal population. Finally the output of the model is the voltage trace $e(t)$ which is proportional to the over all postsynaptic current in the pyramidal cell population and is assumed to be representative of the EEG traces of the overall local area.

The Wendling model has a set of tunable parameters. The constants $d_{m,n}$ and $c_{m,n}$ denote the inhibitory and excitatory connection strengths, respectively, originating from population m to population n and $(m,n) \in$ {p:pyramidal, e:excitatory interneuron, f: fast interneuron, s: slow interneuron}. For a given set of fixed parameters, solutions to the above nonlinear system produce oscillatory behavior that change

little in character regardless of the input. In other words, the oscillations can approximate normal background EEG, sporadic spikes, slow rhythmic activity, and sustained discharge of seizure like spikes. In particular, a change in the balance of slow-to-fast inhibition was shown to move the output from normal to sporadic spikes and into sustained slow quasi-sinusoidal epileptic activity.

2.2 Induced-seizure Model

The model introduced above exhibit fixed oscillatory behavior that depends on the connection parameters, but not the excitatory drive. That is, the dynamics of the nonlinear system demonstrate single stable solutions that depend on the parameter set. As such, it is well suited to model spontaneous seizures caused by functional imbalance in the local population, but not those seizures which are dictated by overwhelming excitatory drive such as those occurring under ECT.

2.2.1 Local Model

We here introduce a simple modification of the local area model that is (i) physiological in nature, and (ii) allows the switch into seizure activity under excessive inputs. Specifically, we propose that dendritic targeting slow inhibitory (GABA-A) interneurons are inhibited for short periods of time upon the arrival of high afferent activity such as that occurring under ECT stimulation. Further, this inhibition is mediated by the fast inhibitory population that primarily targets the somatic regions of pyramidal cells. The overall effect is therefore a transient increase in somatic but a decrease in dendritic inhibition in the target pyramidal cells. This allows excessive excitation buildup in the dendrites and a period of runaway activity to occur in the pyramidal cells before being limited by now-delayed slow inhibitory action. This is motivated by the following :

a) A number of experimental and computational models suggested that impaired dendritic inhibition may play in important role in spontaneously occurring seizures. Using data from five patients to fit Wendling models, it was noted that seizure onsets were consistently characterized by a sudden drop in the dendritic slow inhibition (Wendling et al., 2005). Furthermore, in the period leading to seizure onset (preonset), fast inhibitory activity exhibited a significant increase, which is in line with more evidence suggesting fast activity as instrumental in local ictogenesis (De Curtis and Gnatkovsky, 2009). Slice experiments also point to drastic increases in FS interneuron firing onto pyramidal cells prior to an ictal event at which point these interneurons underwent depolarization block (Cammarota et al., 2013) and a collapse in the inhibitory veto gave way to excitatory runaway (Trevelyan and Schevon, 2013).

b) Recent studies of dendritic targeting interneurons have shown reciprocal connectivity with networks of fast spiking interneurons in the middle cortical layers (Beierlein et al., 2003) or upper cortical layers (Cruishank et al., 2012; Markram et al., 2004). Such networks have distinct functional role and laminar excitation (Katzel et al., 2011), preferential inhibitory targets among inhibitory neuron subtypes (Pfeffer et al., 2013), with somatic targeting fast spiking interneurons firing mediating rapid inhibition of local pyramidal cells (Avermann et al., 2012). Population of slow GABA-A inhibitory cells can be targeted by fast spiking cells (Staiger et al., 1997; Tamás et al., 2004), as reviewed in (Palmer et al., 2012).

Accordingly, the local area model is modified to include a fast inhibitory to slow inhibitory neuron connection (figure 3, green line) with the corresponding change in the dynamics of slow interneurons (equation 5)

$$\dot{x}_{is}(t) = z_3(t) \tag{9}$$
$$\dot{z}_3(t) = Bbd_{sp}S\{c_{ps}x_p(t) - d_{fs}x_{if}\} - 2bz_3(t) - b^2x_{is}$$

2.2.2 Multi-area Model

We here present the network model which accounts for multiple interacting neural populations. The aim is to allow one area to (i) initiate a seizure based solely on external inputs (primary excitatory input, or $u(t)$ in figure 4), and (ii) initiate a feedback excitatory connection with other activated areas which, when driven with inputs that are below seizure threshold, can still lead to an overall network-driven seizure activity. In

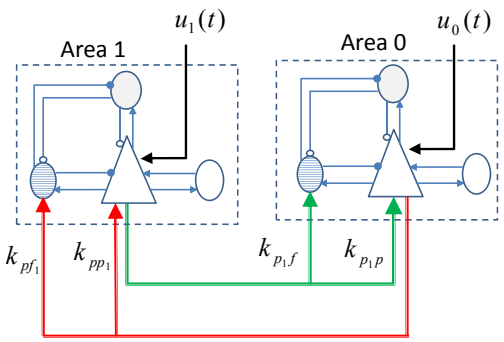

Figure 4: Multi-area model.

the multiarea model, pyramidal populations are assumed to be reciprocally connected (simulating corticortical long range excitatory connections). Furthermore, and as argued in point (b) above, the local fast inhibitory interneuron is proposed to provide feedforward inhibition of pyramidal cell population, thereby "sampling" the afferent long range input arriving onto the pyramidal cell population from other populations. Accordingly, equations 6 and 4 are updated as follows

$$\begin{aligned}\dot{z}_2(t) &= Aa\,[u_0(t)+c_{ep}S\{c_{pe}x_p(t)+k_{p_1p}x_{p1}(t)\}] \\ &\quad -2az_2(t)-a^2x_e \qquad (10)\\ \dot{z}_4(t) &= Ggd_{fp}S\{c_{pf}x_p(t)+k_{p_1f}x_{p1}(t)-d_{sf}x_{ii}(t)\}) \\ &\quad -2gz_4(t)-g^2x_{if} \qquad (11)\end{aligned}$$

where $x_{p1}(t)$ is the synaptic current associated with pyramidal cells in area 1, and k_{p_1f} is a long range excitatory input to local fast inhibitory cell.

2.3 Simulated Seizure Induction

The oscillatory characteristic of the introduced multi-area model is studied with respect to the role of local fast-to-slow inhibition d_{fs}, the long range connections from area 1 to area 0 (denoted as k_{p_1p}, k_{p_1f}), as well as from area 0 to area 1 (denoted as k_{pp_1}, k_{pf_1}). Finally, the effect of the strength of external stimuli arriving at both areas $u_0(t)$,$u_1(t)$ on seizure initiation is presented. In all the simulations below, various parameters other than those presented were fixed at values which allow normal background activity under no external input (see (Wendling et al., 2002)).

The EEG output of the model can vary between four basic states, background normal EEG, normal EEG interrupted by sporadic spikes, sustained slow oscillations, and seizures, as shown in figure 5. In what follows we will study the effect of various parameters, particularly those that were modified, on the initiation of seizures under external stimulation.

Role of Local Fast-to-Slow Inhibition d_{fs}. The critical effect of this local inhibitory connection between fast and slow interneurons is demonstrated in figure 6. Here, it is seen that for nonzero values of d_{fs}, the input threshold for inducing sustained oscillations and seizure activity drops significantly. For $d_{fs} < 5$, a normal EEG rhythm can be obtained at low values of external input $u_0(t) < 50$Hz which will be transformed to sustained oscillations for $u_0 < 200$Hz and then seizure for larger u_0. At larger values of $d_{fs} > 10$, the network will produce sustained oscillations at low input strengths. Hence, normal multi-modal operation of this system implicates a range of $0 < d_{fs} < 5$.

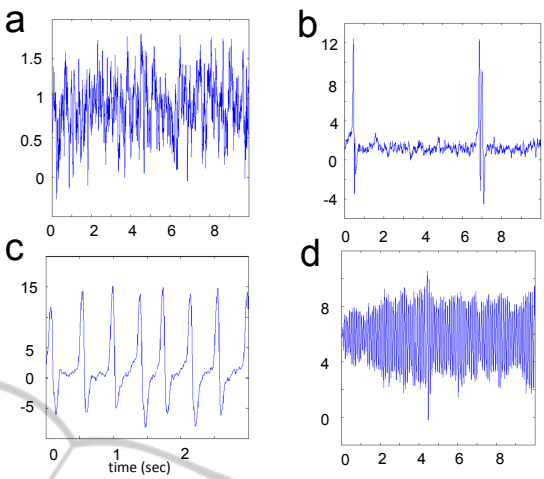

Figure 5: Various EEG patterns produced by the multi-area model. a) Background activity. b) Sporadic spikes. c) Sustained slow oscillations. d) Seizures.

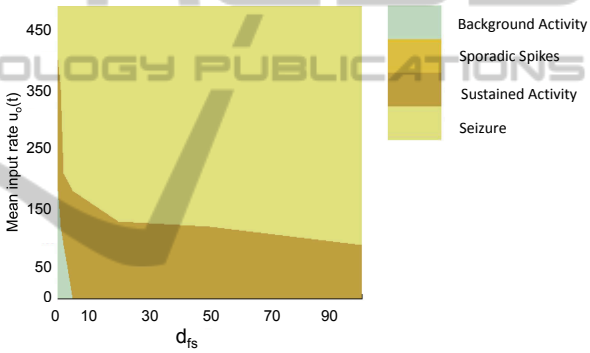

Figure 6: Effect of local fast-to-slow inhibitory connection. Range of input strength is selected to compare the network threshold for seizure induction under assumed connection strengths.

Mechanism of Seizure Induction. To understand why the fast-to-slow inhibition reduced seizure threshold with external input, we note that slow inhibition, which targets the dendritic region of pyramidal cells, has the important role of reducing excitation arriving in the dendritic tree of these cells. Under normal operation, slow inhibition peaks slightly after afferent excitation to pyramidal cells(time constants in the range of 200 and 100 msec, respectively), and sustains a balanced state of operation. The suprathreshold activation of fast inhibitory cells by external inputs will quickly activate the fast-to-slow inhibition(time constant ∼20 msec), thus delaying the dendritic inhibition and providing a time window of runaway excitation in pyramidal cells. The cycle will repeat after the now-delayed dendritic inhibition is reduced to baseline levels.

Role of Long Range Connections. We will now test the ability of long-range connections to induce and propagate seizures between two reciprocally connected areas. Throughout, the strength of local fast-to-slow inhibition is set to $d_{fs} = 2$. Considering the situation where area 0 has normal driving input (that which creates a normal background EEG, $u_0 = 90$ Hz), we will increase (i) excitation to connected area 1, (ii) long range inhibitory connection strength k_{pf} and study the state of area 0 as the excitatory connections k_{p_1p} and k_{pp_1} are varied. This is shown in figure 7.

In the case of low external input to area 1 ($u_1 = 90$ Hz), normal operation is observed for excitatory connection strength $k_{p_1p} < 50$, $k_{pp_1} < 50$ (region bounded by $0 < k_{p_1p} + k_{pp_1} < 50$). This is true regardless of whether long range inhibition is absent (Figure 7, a; $k_{p_1f} = 0$) or present (Figure 7, c; $k_{p_1f} = 100$,$k_{pf_1} = 25$).

In the case of higher external input to area 1 ($u_1 = 180$ Hz) as would be expected with ECT stimuli, and in the absence of long range inhibition $k_{p_1f} = k_{pf_1} = 0$, normal operation persist in area 0 as long as area 1 to area 0 pyramidal connectivity is small $k_{p_1p} < 5$ (figure 7, b). It is only when moderate Pyramidal-Pyramidal connectivity $k_{p_1p} < 30$ occurs that slow oscillations in area 0 can be observed. Nevertheless, area 0 seizures are not observed in this case

The situation changes considerably when long-range inhibition is included (figure 7, d, $k_{p_1f} = 100$, $k_{pf_1} = 25$). In this case, slow oscillations occur even for negligible Pyramidal-Pyramidal connections. Moreover, for seizures to be induced, it is sufficient that modest increases occur in either feedforward or feedback connection ($k_{p1p} > 50$ or $k_{pp_1} > 50$).

To summarize, the presence of long-range pyramidal to inhibitory connection is seen not to induce seizure activity under normal nonreciprocal Pyramidal-Pyramidal connections (only when both reciprocal, feedforward and feedback, connections are large that seizures occur; figure 7,c). Furthermore, such connection promotes the generation of seizures under modest increases in stimulation of one area when the two areas are connected in either feedforward or feedback fashion.

3 CUBATURE KALMAN FILTER

In this section we employ recursive estimation techniques to estimate the parameters of the model introduced in Section 2. Given a set of measurements, we utilize a Kalman-filtering based technique to estimate the parameters in an efficient and recursive way.

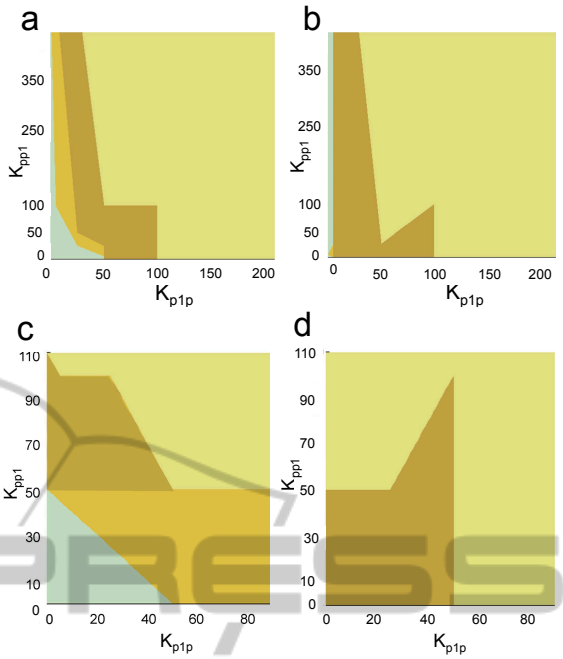

Figure 7: Effect of long-range inhibitory activation. Shown is the state of area 0 ($u_0 = 90$ Hz). a) :$u_1 = 90$, $k_{p_1f} = k_{pf_1} = 0$, b): $u_1 = 180$, $k_{p_1f} = k_{pf_1} = 0$. c):$u_0 = 90$, $u_1 = 90$, $k_{p_1f} = 100$, $k_{pf_1} = 25$ d): $u_1 = 180$, $k_{p_1f} = 100$, $k_{pf_1} = 25$.

This is the cubature Kalman filter that is able to efficiently estimate hidden nonlinear dynamics with the assumption of Gaussian driving noise (Arasaratnam and Haykin, 2009). Additionally, the technique will allow us to estimate the evolution of the states with time. Using a Kalman filter of an appropriate type has been used in contexts similar to ours, particularly in estimating fMRI connectivity in (Havlicek et al., 2011).

3.1 Discrete-time Model

Since the measurements at hand are taken (and stored) at regular intervals, they inherently form a discrete-time process. The first step is to sample the continuous-time model we developed yielding governing equations that take the general form:

- The "process equation" (Wendling model):

$$\mathbf{x}[k] \quad = \quad f(\mathbf{x}[k-1], u_0[k-1])$$

  where $\mathbf{x}[k]$ is the state vector, the elements of which are the k-sampled values of the various state variables $(x_p(\cdot), x_e(\cdot), \cdots)$, $u_0[k]$ is the k-sampled value of in the input $u_0(\cdot)$ and $f(\cdot,\cdot)$ is a *non-linear* function.

- The "measurement equation" (the difference between the states):

$$e[k] \quad = \quad h(\mathbf{x}[k]) + \omega[k],$$

Table 1: CKF Pseudocode.

Initialization:
Set an initial estimate for mean of covariance matrix
Set the initial cubature points
Prediction:
Evaluate the time-prediction cubature points
Propagate these points through the function $f(\cdot,\cdot)$
Estimate the state as a weighted mean
Estimate the covariance matrix
Update:
Evaluate the update cubature points
Propagate these points through the function $h(\cdot)$
Update the state estimate as a weighted mean
Update the covariance matrix

where $e[k]$ is the kth sample value of the measurement signal $e(\cdot)$, $\omega[\cdot]$ is the measurement noise process and $h(\cdot)$ is a linear operator.

Next, we augment the state vector to include the parameters to be estimated and adjust the process and measurement equations accordingly. Since the resulting formulation is non-linear, a square-root cubature Kalman filter was preferred as it offered noticeable numerical stability over the standard cubature Kalman filter. Table 1 presents a pseudocode for the filtering steps.

3.1.1 Multiarea Network Example

Here we present the results of estimating a surrogate EEG data created by simulating a 4-area network model (figure 8). For simplicity, all the areas in the network are assumed to be reciprocally connected. Further, we assume that all the connection parameters of the network are known except for the long-range connections emanating from *area 2* (both excitatory and inhibitory). For this example, the connection parameters are as follows $k_{p_1p_2} = k_{p_1p_3} = k_{p_1p_4} = 30$, $k_{p_3p_1} = k_{p_3p_2} = k_{p_3p_4} = 20$, $k_{p_4p_1} = k_{p_4p_2} = k_{p_4p_3} = 20$. The corresponding inhibitory connections are half of those listed (e.g. $k_{p_1f_2} = k_{p_1p_2}/2 = 15$). Finally, individual areas local connectivity was set to be the same for all areas with $d_{fs} = 1$. For the stimulus, we assumed that the major ECT-like stimulus arrives onto *area 1* while significantly smaller stimuli arrive to the remaining three areas. The activity in *area 1* subsequently recruits the other areas via the long-range reciprocal connections. Numerically, we assume $u_i(t) = u_i * p(t) + n(t)$ where $p(t)$ is a repeating pulses of width=0.5 sec at intervals of 1 sec, $n(t)$ is a random white noise component with zero mean and variance 10 Hz (keeping $u_i(t) \geq 0 \forall t$); finally u_i is a magnitude for area i, with corresponding strengths $u_1 = 150$ Hz, $u_2 = u_3 = u_4 = 60$ Hz.

The resultant simulated EEG traces over the four areas are shown in (figure 9, top). It is seen here that *area 1* precedes the other areas into slow spike-and-wave form of seizure much like that seen in actual data (figure 9, bottom). Note that the real EEG data is added here for qualitative comparison purposes only and was not used to estimate connectivity for that experiment (work in progress). To verify the performance of the estimator, we can estimate based on the simulated EEG traces the (assumed unknown but constant) connectivity of *area 2* to the other areas $k_{p_2p_i} = k_{p_2p_1}$, $i = \{1,3,4\}$. Based on the applied cubature filter, the estimated EEG is very similar to the simulated one (not shown). In this example, only area 2 connectivity $k_{p_2p_1}$ was unknown while other connectivity strengths were assumed fixed. It is seen that, starting from an initial significantly different strength ($k_{p_2p_1} = 10$), that the estimate over time becomes very close to the values actually used in the simulation ($k_{p_2p_1} = 60$, figure 10; note that the inhibitory connection k_{p2f_i} was also unknown but fixed at half $k_{p_2p_i}$,$i = \{1,3,4\}$). The choice of initial value, in this instance, did not affect the performance of the estimator, particularly that the model output is sensitive to this parameter and the cubature filter is reported to be more robust than other nonlinear estimators(see below).

Performance Constraints in Kalman Filtering. The cubature Kalman filter is a powerful tool for nonlinear dynamic system state and parameter estimation under Gaussianity assumptions. A thorough evaluation of its improved stability and convergence properties when compared to earlier nonlinear estimators (unscented Kalman) have been reported in the literature (Arasaratnam and Haykin, 2009). The CKF performance has also been compared with another recently introduced Bayesian approaches (dynamic expectation maximization DEM) on benchmark examples (Havlicek et al., 2011) and was found to be produce improved performance particularly in terms of less sensitivity to initial conditions and noise covariance.

Kalman filtering techniques have been used in several neural modeling applications. Unscented Kalman filters were used in assimilating data related to nonlinear dynamics of sleep rhythms in the brain (Sedigh-Sarvestani et al., 2012), and of spontaneous seizures(Ullah and Schiff, 2010). Cubature Kalman filters were used to estimate neural dynamics from functional imaging data (Havlicek et al., 2011).

In the current simulation/estimation approach for ECT induced seizures, the CKF was used to estimate hidden state vector augmented to include both neural

firing states and inter-areal connectivity parameters. Obviously, the ability to estimate a specific parameter using Kalman filtering is limited by the observability of that parameter at the output as well as the sensitivity of the solution to initial parameter values (for review, see (Sedigh-Sarvestani et al., 2012)). With this in mind, it is important to note that the neural firing models utilized herein are based on an initial set of known local connectivity parameters that produce normal EEG rhythms at the single area level. During estimation, the augmented state vector included those inter-areal connectivity parameters that were noted to affect the switch in simulated EEG from normal to seizure-like patterns. Accordingly, the CKF is intended as a core nonlinear estimator that allow for testing and validating in a stepwise manner various competing models with different parameters acting to produce a given induced seizure rhythm.

3.2 Conclusions

The current paper advocates the use of combined modeling and estimation in understanding the generation and propagation of ECT induced seizures between cortical areas. This effort is intended to be a first step of an ongoing larger modeling framework that includes both the passive head conduction and active neural propagation. Our long-term aim is to introduce computationally efficient models of ECT induction that are both sufficiently accurate and are amenable to incorporation to an ECT optimization tool whereby electrode location and stimulus nature are varied to minimize ECT side effects while preserving ECT efficacy in treating depression. To our knowledge, this is the first effort in modeling ECT seizure generation at the active tissue level using well-identified cortical cells. As mentioned in the introduction, earlier work have primarily focused on the volume conduction properties of a passive head model at increasing geometric and conductivity realism of scalp-skull-brain media. As for seizure initiation, the neural activeness is either mapped to a static threshold function (translated stimulation current to a membrane potential (Deng et al., 2011)), or recently as a homogenous excitable neural medium with no identifiable cortical cellular populations (Bai et al., 2012).

It is important here to note that the proposed model is intended to simulate externally induced seizures in models of normal cortical operation and is thus significantly distinct from the plethora of models that simulate spontaneously occurring seizure phenomena in pathological cortical operation. Furthermore, and while numerous animal and experimental studies have been conducted to understand the key players in electrogenesis of spontaneous seizures, similar studies on externally (ECT) induced seizures are largely missing (for potential mechanism of ECT efficacy at the system level see (Sanchez et al., 2009)) and limited to imaging (fMRI/SPECT) rather than electrophysiological (surface/depth EEG) (cf (Enev et al., 2007; Takano et al., 2011) and references therein).

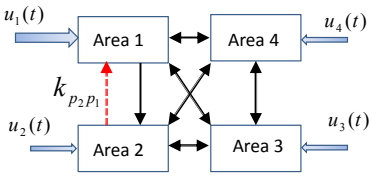

Figure 8: Simulated network.

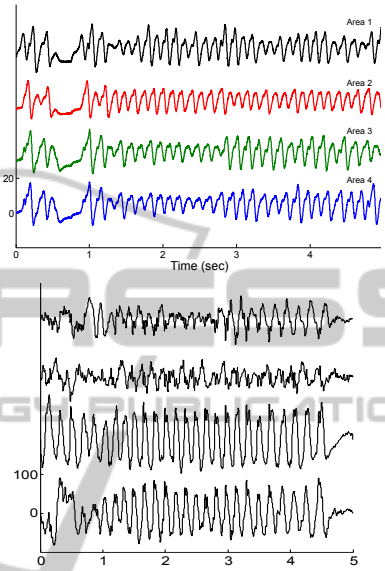

Figure 9: Top:Simulated EEG traces. Bottom: Experimental EEG recordings during an ECT session(band pass filtered between 2 and 30 Hz).

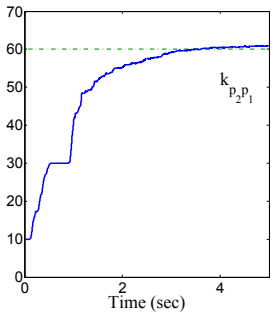

Figure 10: Performance of the CKF. Time evolution of the estimated excitatory connectivity parameter k_{p2p_i} in the 4-area simulated network shown in figure 8 (dotted line=actual value).

Our approach is similar to spontaneous EEG modeling efforts that recently emerged and incorporated head-brain active models in an attempt to explain spontaneous EEG rhythms. Still, such models were either hand-tuned and did not incorporate a joint modeling-estimation modules as proposed herein, or are computationally intensive. The current manuscript advocates simple population-level model that (a) allow emergent ECT-induced seizures from normal operation conditions, (b) are biologically plausible since they derive from neurophysiological evidence, and (c) are computationally favorable since they employ generalized cortical population models and have few fixed parameters (to significantly modify behavior from normal to epileptic EEG), thereby making them amenable to estimation.

It also demonstrated the utility of a general nonlinear estimation framework in estimating the connection strengths based on real ECT seizure data. This is an integral component to simulate and understand how seizures propagate among cortical areas under stimulation. The development of such biologically plausible models carries the long-term potential of developing and designing improved ECT-stimulus delivery configurations that will (a) retain ECT therapeutic efficacy and (b) reduce cognitive side-effects of associated epilepsies. The preliminary results introduced here focused on the potential role of cortical inhibition particularly, inhibition of inhibition, in promoting seizures. It is suggested that commonly reported fast activity at seizure onsets can actively contribute to seizure generation (before depolarization block) by inhibiting dendritic-targeting interneurons thus disinhibiting local pyramidal cells. Other commonly reported global and local players in induced epileptogenesis are to be addressed in more elaborate models. These include thalamocortical interactions (Demont-Guignard et al., 2012), slow synaptic mechanisms such as presynaptic GABA-B receptors activation (Dugladze et al., 2013), accumulation of Cl^- within the intracellular pyramidal cell membrane under excessive stimulation, and possibly astrocyte-neuron cell interactions.

The estimation framework, an augmented state cubature Kalman filter, was shown to behave reasonably well on a set of simulated EEG traces intended to approximate induced seizures. While the augmented state vector here included only one parameter, our ongoing work intends to estimate multiple connectivity parameters from real EEG recordings obtained from ECT-induced seizures and subsequently verify the connection topology with known propagation patterns of seizures in experimental setup. As mentioned earlier, the employment of cubature Kalman filtering for parameter estimation could suffer from lack of accuracy particularly for those parameters that are not observable at the output. Since our choice of model starts with an initial parameter set that allows produces normal EEG behavior, only between-area connectivity was estimated, as output-observable parameters, to fit the EEG transition into induced seizures.

ACKNOWLEDGEMENTS

Project supported by the National Council for Scientific Research, Lebanon (LNCSR) and by the AUB Farouk Jabre Interfaculty Award.

REFERENCES

Arasaratnam, I. and Haykin, S. (2009). Cubature kalman filters. *Automatic Control, IEEE Transactions on*, 54(6):1254–1269.

Avermann, M., Tomm, C., Mateo, C., Gerstner, W., and Peterson, C. (2012). Microcircuits of excitatory and inhibitory neurons in layer2/3 of mouse barrel cortex. *Journal of Physiology*, 107(11):175–191.

Bai, S., Loo, C., Al Abed, A., and Dokos, S. (2012). A computational model of direct brain excitation induced by electroconvulsive therapy: comparison among three conventional electrode placements. *Brain Stimulation*, 5(3):408–421.

Beierlein, M., Gibson, J. R., and Connors, B. W. (2003). Two dynamically distinct inhibitory networks in layer 4 of the neocortex. *Journal of neurophysiology*, 90(5):2987–3000.

Cammarota, M., Losi, G., Chiavegato, A., Zonta, M., and Carmignoto, G. (2013). Fast spiking interneuron control of seizure propagation in a cortical slice model of focal epilepsy.

Cruishank, S., Ahmed, O., Stevens, T., Patrick, S., Gonzalez, A., Elmaleh, E., and Connors, B. (2012). Thalamic control of layer 1 circuits in prefrontal cortex.

De Curtis, M. and Gnatkovsky, V. (2009). Reevaluating the mechanisms of focal ictogenesis: The role of low-voltage fast activity. *Epilepsia*, 50(12):2514–2525.

Demont-Guignard, S., Benquet, P., Gerber, U., Biraben, A., Martin, B., and Wendling, F. (2012). Distinct hyperexcitability mechanisms underlie fast ripples and epileptic spikes. *Annals of Neurology*, 71:342–352.

Deng, Z.-D., Lisanby, S. H., and Peterchev, A. V. (2011). Electric field strength and focality in electroconvulsive therapy and magnetic seizure therapy: a finite element simulation study. *Journal of neural engineering*, 8(1):016007.

Dugladze, T., Maziashvili, N., Börgers, C., Gurgenidze, S., Häussler, U., Winkelmann, A., Haas, C. A., Meier, J. C., Vida, I., Kopell, N. J., et al. (2013). Gabab autoreceptor-mediated cell type-specific reduction of

inhibition in epileptic mice. *Proceedings of the National Academy of Sciences*, 110(37):15073–15078.

Enev, M., McNally, K. A., Varghese, G., Zubal, I. G., Ostroff, R. B., and Blumenfeld, H. (2007). Imaging onset and propagation of ect-induced seizures. *Epilepsia*, 48(2):238–244.

Havlicek, M., Friston, K. J., Jan, J., Brazdil, M., and Calhoun, V. D. (2011). Dynamic modeling of neuronal responses in fmri using cubature kalman filtering. *Neuroimage*, 56(4):2109–2128.

Jansen, B. H. and Rit, V. G. (1995). Electroencephalogram and visual evoked potential generation in a mathematical model of coupled cortical columns. *Biological cybernetics*, 73(4):357–366.

Katzel, D., Zemelman, B., Buetfeing, C., Wolfel, M., and Miesenbock, G. (2011). The columnar and laminar organization of inhibitory connections to neocortical excitatory cells.

Lee, W. H., Deng, Z.-D., Kim, T.-S., Laine, A. F., Lisanby, S. H., and Peterchev, A. V. (2012). Regional electric field induced by electroconvulsive therapy in a realistic finite element head model: Influence of white matter anisotropic conductivity. *Neuroimage*, 59(3):2110–2123.

Markram, H., Rodrequez, M., Wang, Y., Gupta, A., and Wu, C. (2004). Interneurons of the neocortical inhibitory system.

Merkl, A., Heuser, I., and Bajbouj, M. (2009). Antidepressant electroconvulsive therapy: mechanism of action, recent advances and limitations. *Experimental neurology*, 219(1):20–26.

Palmer, L., Murayama, M., and Larkum, M. (2012). Inhibitory regulation of dendritic activity in vivo. *Frontiers in neural circuits*, 6.

Pfeffer, C. K., Xue, M., He, M., Huang, Z. J., and Scanziani, M. (2013). Inhibition of inhibition in visual cortex: the logic of connections between molecularly distinct interneurons. *Nature neuroscience*, 16(8):1068–1076.

Sackeim, H. A., Prudic, J., Nobler, M. S., Fitzsimons, L., Lisanby, S. H., Payne, N., Berman, R. M., Brakemeier, E.-L., Perera, T., and Devanand, D. (2008). Effects of pulse width and electrode placement on the efficacy and cognitive effects of electroconvulsive therapy. *Brain Stimulation*, 1(2):71–83.

Sanchez, R., Alcoverro, O., Pagerols, J., and Rojo, J. (2009). Electrophysiological mechanisms of action of electroconvulsive therapy. *Actas Esp Psiquiatr*, 37(6):343–351.

Sedigh-Sarvestani, M., Schiff, S. J., and Gluckman, B. J. (2012). Reconstructing mammalian sleep dynamics with data assimilation. *PLoS computational biology*, 8(11):e1002788.

Staiger, J. F., Freund, T. F., and Zilles, K. (1997). Interneurons immunoreactive for vasoactive intestinal polypeptide (vip) are extensively innervated by parvalbumin-containing boutons in rat primary somatosensory cortex. *European Journal of Neuroscience*, 9(11):2259–2268.

Takano, H., Motohashi, N., Uema, T., Ogawa, K., Ohnishi, T., Nishikawa, M., and Matsuda, H. (2011). Differences in cerebral blood flow between missed and generalized seizures with electroconvulsive therapy: A positron emission tomographic study. *Epilepsy research*, 97(1):225–228.

Tamás, G., Szabadics, J., Lörincz, A., and Somogyi, P. (2004). Input and frequency-specific entrainment of postsynaptic firing by ipsps of perisomatic or dendritic origin. *European Journal of Neuroscience*, 20(10):2681–2690.

Trevelyan, A. J. and Schevon, C. A. (2013). How inhibition influences seizure propagation. *Neuropharmacology*, 69:45–54.

Ullah, G. and Schiff, S. J. (2010). Assimilating seizure dynamics. *PLoS computational biology*, 6(5):e1000776.

Wendling, F., Bartolomei, F., Bellanger, J., and Chauvel, P. (2002). Epileptic fast activity can be explained by a model of impaired gabaergic dendritic inhibition. *European Journal of Neuroscience*, 15(9):1499–1508.

Wendling, F., Hernandez, A., Bellanger, J.-J., Chauvel, P., and Bartolomei, F. (2005). Interictal to ictal transition in human temporal lobe epilepsy: insights from a computational model of intracerebral eeg. *Journal of Clinical Neurophysiology*, 22(5):343–356.